Experimental Studies of Power-Saturated Spin Modes of Nitroxides in Liquids 1

Barney L. Bales[1], Miroslav Peric[1], and Robert N. Schwartz[2]

[1] Department of Physics and Astronomy, California State University at Northridge, Northridge, CA, 91330, USA
[2] Electrical and Computer Engineering Department, University of California, Los Angeles, Los Angeles, CA90095, USA.

Abstract

In recent years, the theory of the effect of saturation of EPR spectra of free radicals undergoing spin exchange has been extended to spin exchange frequencies where "peculiar" behavior occurs. In a paper by Salikhov (Appl. Magn. Reson. (2021) 52:1063–1091), analytic expressions were developed that predict the dependence of measurable EPR parameters on the exchange frequencies and the microwave field strength. This work is an experimental test of that theory where, in principle, there are no adjustable parameters.

Dedicated to Professor James D. Currin (1931 – 2017) whose theory of Heisenberg Spin Exchange in 1962 for unsaturated spectra of free radicals in liquids holds up to this day.

1 Introduction

We learned already in 1962 that the EPR spectrum of a free radical undergoing Heisenberg spin exchange (HSE) showed a dispersion (DIS) signal in addition to the "normal" absorption of energy (ABS) [1]. It was recognized that the study of HSE was an ideal method to investigate bimolecular collisions in liquids, a fact that stimulated the rapid development of the field: see [2, 3] and references therein for a historical survey and [4] for a comprehensive, modern treatment of the subject as applied to nitroxide free radicals (nitroxides). This work is limited to ^{15}N nitroxides. All spectra are in the fast-mobility regime presented as first-derivatives with respect to the swept external magnetic field. The DIS component was largely ignored or avoided in the case of ^{14}N by studying the center-field line, (cf), until 1980 when a comprehensive monograph devoted to HSE was published in English [2]. At that time, DIS was recognized to render the resonance line non-Lorentzian; however, it was not used to study the spin exchange frequency, ω_{ex}, until 1997 [3]. DIS was treated with perturbation theory in [2] where $\omega_{ex} \ll \gamma A_0$. A_0 (G) is the ^{15}N or ^{14}N isotropic coupling constant for $\omega_{ex} \to 0$ and γ the gyromagnetic ratio of the electron. In the slow exchange regime, DIS increased linearly with ω_{ex} [2]. As expected, as $\omega_{ex}/\gamma A_0$ increased, the perturbation theory result was found to be inadequate to interpret experimental results [5]; however, allowing the amplitude of DIS to increase non-linearly with ω_{ex} led to good agreement. In 2002 [5], it was proposed that each line was the superposition of only one ABS and one DIS for all values ω_{ex} based on experimental evidence [5]. This conjecture was later confirmed numerically [6] and theoretically [7].

In [7], Salikhov proposed a new, important view of the effect of HSE on EPR spectra for unsaturated ^{15}N nitroxides, that established that the two lines are collective states of two sub-

ensembles of spins, referred to as *spin modes*, and each is composed of only one ABS and one DIS.

Until 2017 [8], most studies of HSE were limited to unsaturated spectra; i.e., $H_1^2\gamma^2 T_1 T_2 \ll 1$, where H_1 is the circularly polarized magnetic induction of the microwave field [9]. For $H_1 \to 0$, Salikhov [7] derived eqs 1 – 3 valid for all $\omega_{ex} < \gamma A_0$ as follows:

$$\omega_{ex}/\gamma A_0 = \left\{ \left[\left(\frac{4}{3\sqrt{3}} \right) \Big/ \left(\frac{V_{disp}}{V_{pp}} \right)_0 \right]^2 + 1 \right\}^{-1/2} \tag{1}$$

$$\omega_{ex}/\gamma A_0 = \sqrt{3} \left\{ \left(\Delta H_{pp}^L \right)_0 - \left[\Delta H_{pp}^L(0) \right]_0 \right\} \tag{2}$$

$$\omega_{ex}/\gamma A_0 = \sqrt{1 - [A_{abs}^2/A_0^2]_0} \tag{3}$$

where the subscripts denote the values as $H_1 \to 0$. The dependence on C is suppressed except that $\left[\Delta H_{pp}^L(0) \right]$ means the limit $C \to 0$. $\left[\Delta H_{pp}^L(0) \right]_0 = 2T_2^{-1}/\sqrt{3}$ [10]. V_{disp}, V_{pp}, ΔH_{pp}^L, and A_{abs} are defined in Fig. 2 of **Results and Discussion** below.

In a series of three papers [9, 11, 12], Salikhov predicted a number of "peculiar" behaviors that had not been tested experimentally. See the SI of [13] for a brief summary of the new predictions.

One such prediction, that A_{abs} would increase with increasing H_1, that Salikhov attributed to the formation of spin polaritons, collective modes between the spin system and the photons, was confirmed qualitatively in [13, 14]. The purpose of the present work is to study the predictions of [9] quantitatively. We find remarkable agreement between theory and experiment over the range of H_1 available with a standard commercial CW EPR spectrometer.

2 Theory

In the presence of spin exchange, Salikhov [9] (in eq 6) derived the matrix $\mathcal{L}$ (Liouville linear operator) which contains terms describing the effects of spin coherence transfer between the two resonance frequencies for a $S = \frac{1}{2}$. $I = \frac{1}{2}$ spin system each of which have the same values of T_1 and T_2. From there, he provided two ways to obtain measurable parameters: (1) from computing and fitting the spectrum or (2) from analytical equations [9]. We have confirmed that both approaches yield identical results. To obtain experimental parameters, fitting the spectrum is the only option. Theoretical parameters may be obtained from either fits of the theoretical spectra or from the analytical forms. The fits are precise, but tedious; thus we use the analytical forms.

Reference [9] provides the theory for this work; for the reader who wishes a broader view of modern HSE theory, see ref. [15].

2.1 Expression for the Spectrum

For given values of T_1 and T_2, the first-derivative spectrum derived from eq 7 of [9] is as follows:

$$Y'(H, \omega_{ex}, H_1) = -\frac{d}{dH}\frac{M_0 \mathcal{R}_1 H_1}{Den}\left\{\mathcal{A}\left[\left(\frac{A_0}{2}\right)^2 \mathcal{B} + \mathcal{R}_2 \mathcal{D}\right] + \mathcal{R}_2 \mathcal{B} H_1^2\right\}, \tag{4}$$

where

$$Den = -\left(\frac{A_0}{2}\right)^4 \mathcal{R}_1 \mathcal{A} - [\mathcal{R}_1(\Delta H^2 + \mathcal{R}_2^2) + \mathcal{R}_2 H_1^2][\mathcal{A}\mathcal{D} + \mathcal{B}H_1^2] +$$
$$\left(\frac{A_0}{2}\right)^2 [2\mathcal{R}_1 \mathcal{A}(\Delta H^2 - \mathcal{R}_2 \mathcal{B}) - (\omega'^2_{ex} + 2\mathcal{R}_1 \mathcal{R}_2 + \omega'_{ex}(\mathcal{R}_1 + \mathcal{R}_2))H_1^2]. \tag{5}$$

Here, $\mathcal{R}_1 = 1/\gamma T_1$, $\mathcal{R}_2 = 1/\gamma T_2$, and $\omega'_{ex} = \omega_{ex}/\gamma = K_{ex}C/\gamma$, all having units G, and where $\mathcal{A} \equiv (\omega'_{ex} + \mathcal{R}_1)$, $\mathcal{B} \equiv (\omega'_{ex} + \mathcal{R}_2)$, $\mathcal{D} \equiv (\Delta H^2 + \mathcal{B}^2)$ and $\Delta H = (H - H_0)$. The derivative is effected numerically. Note that T_1 is the spin lattice relaxation time directly to the lattice, measurable for $C \to 0$.

2.2 Analytical Expressions for the Measurable Parameters

The resonance frequencies are found (in frequency units) as the real part of the complex eigenvalues of the evolution operator $\boldsymbol{\mathcal{L}}$ given in eq (10) of [9] as follows:

$$\omega_\pm = \omega_0 \pm (1/2)^{1/2}Re\{[\mathcal{K}_1 + (\mathcal{K}_2)^{1/2}]^{1/2}\}. \tag{6}$$

Subtracting to obtain the spacing between them and converting to magnetic field units gives:

$$A_{abs} = 2^{1/2}Re\{[\mathcal{K}_1 + (\mathcal{K}_2)^{1/2}]^{1/2}\}, \tag{7}$$

where $\mathcal{K}_1$ and $\mathcal{K}_2$ are expressed as:

$$\mathcal{K}_1 = \{-1/[\mathcal{R}_1(\omega'_{ex} + \mathcal{R}_1)]\}\{\mathcal{R}_1(\omega'_{ex} + \mathcal{R}_1)[-(A_0^2/2) + \omega'^2_{ex} + 2\omega'_{ex}\mathcal{R}_2 + 2\mathcal{R}_2^2]$$
$$+ [2\mathcal{R}_1\mathcal{R}_2 + \omega'_{ex}(\mathcal{R}_1 + \mathcal{R}_2)]H_1^2\}, \tag{8}$$

$$\mathcal{K}_2 = \{-A_0^2 \mathcal{R}_1(\omega'_{ex} + \mathcal{R}_1)(\omega'_{ex} + 2\mathcal{R}_2)[\mathcal{R}_1(\omega'_{ex} + \mathcal{R}_1)(\omega'_{ex} + 2\mathcal{R}_2) + (\omega'_{ex} + 2\mathcal{R}_1)H_1^2]$$
$$+ [\omega'_{ex}\mathcal{R}_1(\omega'_{ex} + \mathcal{R}_1)(\omega'_{ex} + 2\mathcal{R}_2) + \omega'_{ex}(\mathcal{R}_1 - \mathcal{R}_2)H_1^2]^2\}/[\mathcal{R}_1^2(\omega'_{ex} + \mathcal{R}_1)^2].[1] \tag{9}$$

Note that the expression for $\mathcal{K}_2$ (R_2) in eq 9 of [9] has a syntax error. The final bracket '}' in the denominator must be deleted. The final parenthesis that appears in the numerator must be replaced by the bracket '}'.

The expression for ΔH_{pp}^L, eq 11 of [9], is given by the imaginary part of the complex eigenvalues of the evolution operator $\boldsymbol{\mathcal{L}}$:

$$\Delta H_{pp}^L = \frac{2}{\sqrt{6}} Im\{[\mathcal{K}_1 + (\mathcal{K}_2)^{1/2}]^{1/2}\}. \tag{10}$$

The theoretical expression for the dispersion contribution, $(V_{disp}/V_{pp})_{lf}$, for arbitrary H_1, given in eq 36 of [9] is somewhat more complicated with closed form:

$$\left(\frac{V_{disp}}{V_{pp}}\right)_{lf} = -\left(\frac{4}{3\sqrt{3}}\right) \frac{\Delta\omega_{1/2}\{A_0^2 \mathcal{T}\mathcal{U} - 4[\mathcal{T}(\mathcal{P}-\mathcal{U}^2) - \mathcal{U}H_1^2]\mathcal{R}_2\}}{\Omega\left\{A_0^2\mathcal{T}\mathcal{U} + 4\left[\mathcal{T}(\mathcal{P}+\mathcal{U}^2)\mathcal{R}_2 + \mathcal{N}(H_1\mathcal{R}_2)^2\right]\right\}}, \tag{11}$$

where $(V_{disp}/V_{pp})_{hf} = -(V_{disp}/V_{pp})_{lf}$, $\Delta\omega_{1/2} = (1/2)^{1/2} Im\{[\mathcal{K}_1 + (\mathcal{K}_2)^{1/2}]^{1/2}\}$, $\mathcal{T} = (\omega_{ex}' + \mathcal{R}_1)$, $\mathcal{U} = (\omega_{ex}' + \mathcal{R}_2)$, $\mathcal{N} = (1 + \omega_{ex}'/\mathcal{R}_2)$, $\Omega = (\mathcal{P} - \Delta\omega_{1/2}^2)^{1/2}$, $\mathcal{P} = \left(\mathcal{R}_2/2\right)^2 \sqrt{\mathcal{X}}$, with

$$\mathcal{X} = \frac{\{[\mathcal{M}(4 + \mathcal{Q} + 4\,\omega_{ex}'/\mathcal{R}_2) + 4\mathcal{S}][\mathcal{Q} + 4\mathcal{N}(1 + \mathcal{S})]\}}{\mathcal{M}}. \tag{12}$$

In eq 12, $\mathcal{M} = (1 + \omega_{ex}'/\mathcal{R}_1)$, $\mathcal{Q} = (A_0/\mathcal{R}_2)^2$, and $\mathcal{S} = H_1^2/\mathcal{R}_1\mathcal{R}_2$..

The integrated intensity-for $\omega_{ex} < \gamma A_0$, given in eq 38 of [9], has the following form:

$$I \,\alpha\, \frac{\mathcal{M}_0 H_1\{\mathcal{Y}[A_0^2 \mathcal{Z} + 4(\mathcal{P} + \mathcal{Z}^2)\mathcal{R}_2] + 4\mathcal{N}(H_1\mathcal{R}_2)^2\}}{16\Delta\omega_{1/2}\mathcal{P}\mathcal{Y}}, \tag{13}$$

in arbitrary units, $\mathcal{Y} = (\omega_{ex}' + \mathcal{R}_1)$, $\mathcal{Z} = (\omega_{ex}' + \mathcal{R}_2)$.

Note that eqs 6 – 13 were programmed in Excel by one of us and in MATLAB by another, yielding identical results. We have confirmed that for $H_1 \to 0$, Currin's equations [1] are identical to eq 4 both for $\omega_{ex} < \gamma A_0$ and $\omega_{ex} > \gamma A_0$ [1, 6] and the Appendix of [3]. For the peculiar behavior in the regime $\omega_{ex} > \gamma A_0$, see [16] where two ABS are observed experimentally, one positive and the other negative (emissive). The negative signal has been termed the Phantom [16].

3 Materials and Methods

3.1 Materials

Per deuterated 4-oxo-2,2,6,6-tetramethylpiperidine-N-oxyl (pdT) was purchased from CDN Isotopes and the K_2CO_3 from Mallinckrodt and were used as received. 15PADS was synthesized as described in detail in the SI of [13]. Solutions were prepared with Millipore water buffered with 50-mM K_2CO_3.

3.2 Purity of 15PADS

The purity of 15PADS was determined by a new technique that we describe briefly anticipating that the approach may be useful for other purposes. Figure 1 displays the EPR spectrum of a mixture of 1.50-mM pdT (1st, 3rd, and 5th lines) and 1.00-mM 15PADS (2nd and 4th lines) at 295 K.
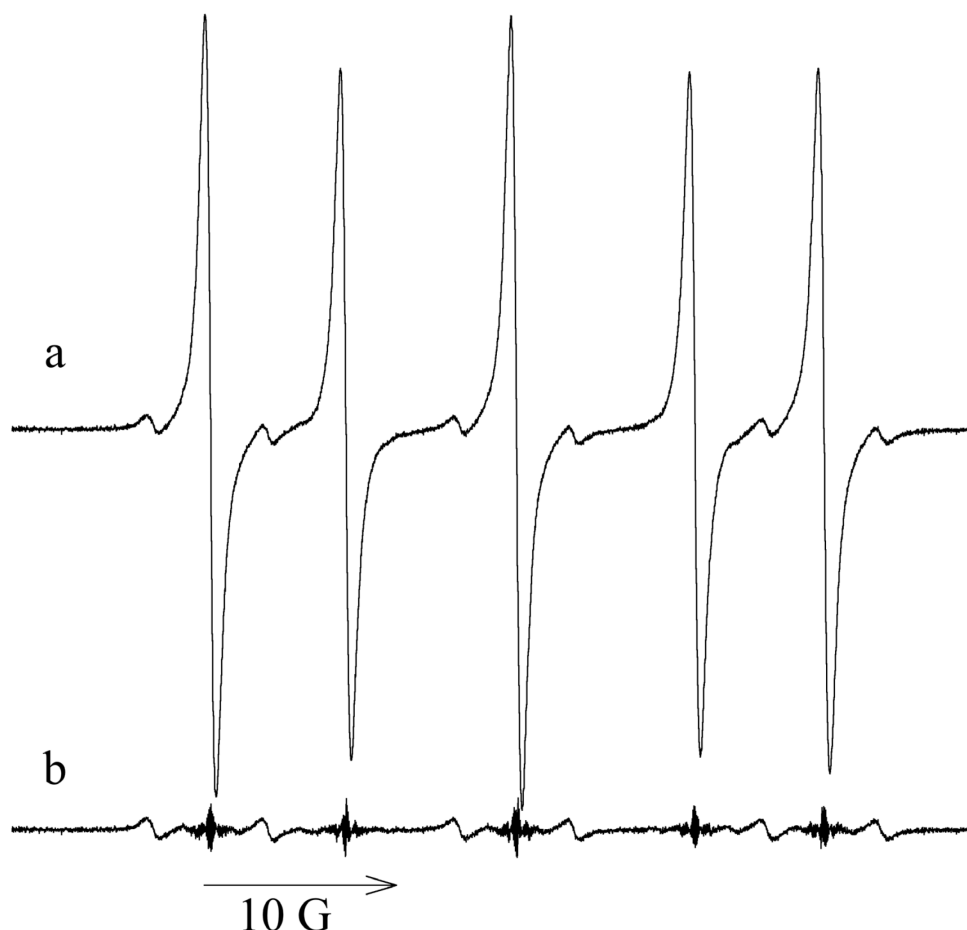

Fig 1 a EPR spectrum of an aqueous mixture of 1.50 pdT (1st, 3rd, and 5th lines) and 1.00 mM 15PADS (2nd and 4th lines) buffered with 50-mM K_2CO_3 at 295 K. $P = 1.26$ mW. The weak lines are due to ^{13}C in natural abundance in pdT. The fit, nearly perfect except for the ^{13}C lines, is not shown for clarity. **b** the residual = spectrum minus the fit.

The weak lines are due to ^{13}C in natural abundance in pdT which are not modeled in the fit, thus they appear in the residuals together with the noise. After decomposing the lines into ABS and DIS with the program Lowfit (see below), the doubly-integrated intensity, I, of ABS for each pdT and 15PADS line was calculated. The lines are well-resolved; however, this is not necessary because Lowfit includes line overlap. Because the ^{13}C lines are not included in the fit, I_{pdT} was increased by 1%, the natural abundance of the isotope. $\langle I_{15PADS} \rangle$ is computed as twice the mean value of the two lines and $\langle I_{pdT} \rangle$ as three times the mean value of the three lines. Normalized to $C = 1.00$ mM and 1.50 mM, respectively, the purity of 15PADS relative to pdT

was computed from the ratio of $3\langle I_{15PADS}\rangle/2\langle I_{pdT}\rangle = 0.856 \pm 0.003$. The uncertainty was computed from the propagated values of the standard deviation (sd) for each isotope which is seen to be negligible. The accuracy of the concentration is limited to that of the pdT, quoted as 1%. In addition to this application to compare numbers of spins, this level of precision could be useful in studies of, for example, (1) different radicals to compare the rotational correlation times in exactly the same experimental conditions, (2) to compare the parameters of a radical associated with an aggregate such as a micelle with another associated with the bulk solvent, or (3) compare a radical with its deuterated counterpart to investigate the intercept discrepancy for partially resolved spectra [17].

3.2 Samples and CW EPR

A 136-mM solution of 15PADS was prepared by weight in aqueous 50-mM K_2CO_3, yielding a nominal concentration of 116 mM taking into account its 85.6 % purity. Samples of lower concentrations were prepared by serial dilution. The samples were deoxygenated by bubbling N_2 gas for 20 minutes through a 5-μL pipette. The same pipette was filled by capillary action to 2/3 full, sealed at each end with Sigillum Wax Sealant (Globe Scientific 51601), and stored under a positive pressure of N_2 gas. This sample preparation was effected twice, in runs called Series 1 and Series 2.

Each sample was inserted into a quartz tube which was transferred quickly to the microwave cavity (ER 4119HS, TE_{011}) of a Buker EMXplus EPR EPR spectrometer where an N_2 gas flow maintained the sample deoxygenated and controlled the temperature to 295 K. The 5000-point spectra were obtained with 100-kHz modulation with an amplitude of 0.1 G, time constant 0.01 ms, and conversion time 1 ms. Continuous wave saturation curves (CWS) were obtained using the 2D-Field-Power routine in Bruker's Xenon software package at 20 power settings. The conversion from power, P, to the magnetic induction of the microwave field, $H_1 = \Gamma\sqrt{Q}\sqrt{P}$, was carried out using a standard line sample of 14PADS extending all of the way through the cavity as detailed in [18] where Q is the Q-value of the cavity and Γ is a constant pertinent to the sample and cavity configurations taking into account microwave-focusing effects of the glassware and the fact that a line- rather than a point-sample is used. This resulted in $\Gamma = 0.0229 \pm 0.0012$ G/W$^{1/2}$. The samples were in 5-μL pipettes, with inside diameter equal to 0.146 mm; therefore, they extend into the microwave electric field by 0.073 mm which affords large values of Q while minimizing heating effects. Employing the known temperature dependence of A_0 of 14PADS [19], the temperature rise at the maximum power of 200 mW was found to be less than 1 K. The Bruker set up affords straightforward measurements of Q; however, only to 2 significant figures. During the course of the experiments 79 values of Q were obtained. By measuring CWS of $\left(\Delta H_{pp}^L\right)_0$ it was determined that the average value <Q> = 7500 ± 600 gave more consistent results than using individual values. Thus, $H_1 = (1.98 \pm 0.13) \sqrt{P}$ G with P in W.

The spectra are decomposed into their ABS and DIS components with the program Lowfit that is described in detail in the SI of [13] together with an instructive example. Briefly, Lowfit separates ABS and DIS and accounts for overlapping lines. For $C < 0.3$ mM, the lines are slightly non-Lorentzian [18]; however, for $C > 0.8$, the most precise fits are Lorentzian. The experimental values of V_{disp}/V_{pp} were corrected for instrumental dispersion as detailed in [8].

4 Results and Discussion

For Series 1, Fig. 2 shows spectra and decomposed components of 116 mM 15PADS at **a** $H_1 = 0.0353$ G and at **d** $H_1 = 0.885$ G. Parameters derived from the components are defined.

The parameters from Fig. 1 are as follows: $\Delta H_{pp}^L =$ **b** 5.674 ± 0.039 G and **c** 7.086 ± 0.064 G; $V_{disp}/V_{pp} =$ **c, b** 0.451 ± 0.009 and **f, e** 0.484 ± 0.009; and $A_{abs} =$ **b** 15.448 ± 0.005 G and **e** 16.776 ± 0.005 G. Values at $H_1 \to 0$: $\left(\Delta H_{pp}^L\right)_0 = 5.68 \pm 0.08$ G, $(A_{abs})_0 = 15.455 \pm 0.007$ G, and $\left(V_{disp}/V_{pp}\right)_0 = 0.452 \pm 0.009$. Note that only one value of V_{disp}/V_{pp} from each spectrum is available because the instrumental DIS must be corrected, e.g. [20].

The results are presented as the ratio of the parameters divided by their values at $H_1 \to 0$ in order to focus on their behavior vs. H_1. This allows greater visual detail because ω_{ex} influences the parameters more than H_1 [9]. To appreciate this point, compare Figs. 2b and 2a in [13].
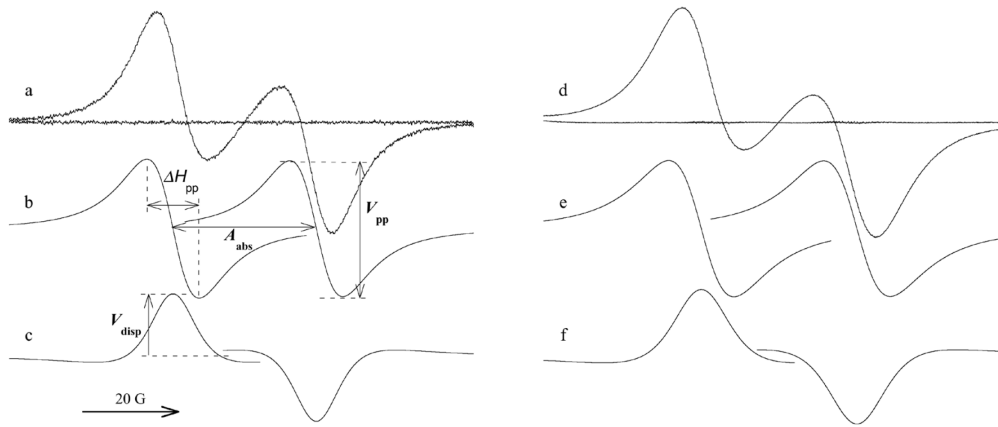

Fig. 2 EPR spectra of a deoxygenated aqueous solution of 116 mM 15PADS of Series 1 at **a** H_1 = 0.0353 G and at **d** H_1 = 0.885 G. The decomposed ABS components are displayed in **b** and **e** and the DIS component in **c** and **f**, respectively. The parameters ΔH_{pp}^L, V_{pp}, V_{disp}, and A_{abs} are defined. The residuals, defined as the spectrum minus ABS + DIS, are displayed along the baselines of **a** and **d**, respectively.

Table 1 details the values of the parameters at $H_1 \to 0$. Table 2 gives the values of ω_{ex}/γ derived from eqs 1 – 3.

Table 1 Parameters at $H_1 \to 0$

C, mM	$\left(\Delta H_{pp}^L\right)_0$, G[a]	$(A_{abs})_0$, G[b]	$\left[V_{disp}/V_{pp}\right]_0$ [b]
		Series 1	
116	5.68 ± 0.08	15.455 ± 0.007	0.452 ± 0.006
98.6	4.64 ± 0.06	16.370 ± 0.006	0.346 ± 0.005
82.6	3.75 ± 0.05	16.976 ± 0.005	0.266 ± 0.004
66.0	2.82 ± 0.04	17.449 ± 0.003	0.190 ± 0.003
49.8	1.99 ± 0.03	17.747 ± 0.002	0.128 ± 0.002
33.3	1.26 ± 0.02	17.916 ± 0.002	0.0753 ± 0.001
18.0	0.69 ± 0.02	17.999 ± 0.001	0.0349 ± 0.001
		Series 2	
116	5.57 ± 0.04	15.808 ± 0.007	0.436 ± 0.006
98.6	4.59 ± 0.03	16.629 ± 0.006	0.337 ± 0.005
82.6	3.74 ± 0.03	17.195 ± 0.004	0.262 ± 0.004
66.0	2.83 ± 0.02	17.652 ± 0.003	0.188 ± 0.003
49.8	2.00 ± 0.02	17.948 ± 0.002	0.126 ± 0.002
33.3	1.27 ± 0.02	18.119 ± 0.001	0.0741 ± 0.001
18.0	0.68 ± 0.01	18.194 ± 0.001	0.0342 ± 0.001

[a] Determined from the CWS of ΔH_{pp}^L fit to eq 9 of [18]. [b] Determined from the CWS of A_{abs} or R_{disp} fit to a quadratic. Uncertainties, fit errors.

Table 2 ω_{ex}/γ, G determined from the parameter in the second row.

C, mM	ω_{ex}/γ, G			
	$\left[\Delta H_{pp}^L(0)\right]_0$, G[a]	$\left[A_{abs}(C)\right]_0$, G[a]	$\left[V_{disp}/V_{pp}\right]_0$ [a]	Average[b]
		Series 1		
116	9.49 ± 0.13	9.26 ± 0.01	9.26 ± 0.10	9.34 ± 0.13
98.6	7.69 ± 0.10	7.53 ± 0.01	7.49 ± 0.09	7.57 ± 0.11
82.6	6.16 ± 0.09	6.04 ± 0.01	5.96 ± 0.07	6.06 ± 0.10
66.0	4.55 ± 0.07	4.50 ± 0.01	4.38 ± 0.06	4.48 ± 0.08
49.8	3.11 ± 0.05	3.12 ± 0.01	3.00 ± 0.04	3.08 ± 0.07
33.3	1.84 ± 0.04	1.92 ± 0.02	1.78 ± 0.03	1.85 ± 0.07
18.0	0.848 ± 0.03	0.849 ± 0.02	0.827 ± 0.01	0.841 ± 0.01
		Series 2		
116	9.31 ± 0.06	9.05 ± 0.01	9.00 ± 0.10	9.12 ± 0.17
98.6	7.62 ± 0.06	7.43 ± 0.01	7.33 ± 0.09	7.46 ± 0.15
82.6	6.14 ± 0.04	6.01 ± 0.01	5.88 ± 0.07	6.01 ± 0.13
66.0	4.56 ± 0.04	4.49 ± 0.01	4.34 ± 0.06	4.46 ± 0.11
49.8	3.13 ± 0.04	3.10 ± 0.01	2.95 ± 0.04	3.06 ± 0.10
33.3	1.85 ± 0.03	1.86 ± 0.01	1.75 ± 0.02	1.82 ± 0.06
18.0	0.845 ± 0.02	0.853 ± 0.020	0.810 ± 0.011	0.836 ± 0.023

[a]Uncertainties, propagated fit error. [b]Average, unweighted means; uncertainties, sd.

For the two series, Series 1 and 2, Fig. 3 shows the peculiar behavior of A_{abs}, increasing as a function of H_1, that Salikhov attributed to the formation of spin polaritons [9]. The solid lines are computed with eq 7 employing $(A_{abs})_0$ taken from Table 1 with $\gamma T_1 = \gamma T_2 = 7 \text{ G}^{-1}$ [21], $A_0 = 18.270$ G and ω_{ex} from column 2 of Table 2 for Series 1. The purpose of employing the values of ω_{ex} from Series 1 for both series and all parameters is to show the systematic discrepancies from different runs and different parameters. Using the values from Series 2, would lower the solid lines for both series rendering the fits in **b** slightly better and those in **a**, slightly poorer. The fits confirm that the theory is correct quantitatively. Note that the uncertainties derived from the fit errors are smaller than the symbols in Fig. 3; thus, apparently there are systematic errors that are difficult to estimate.
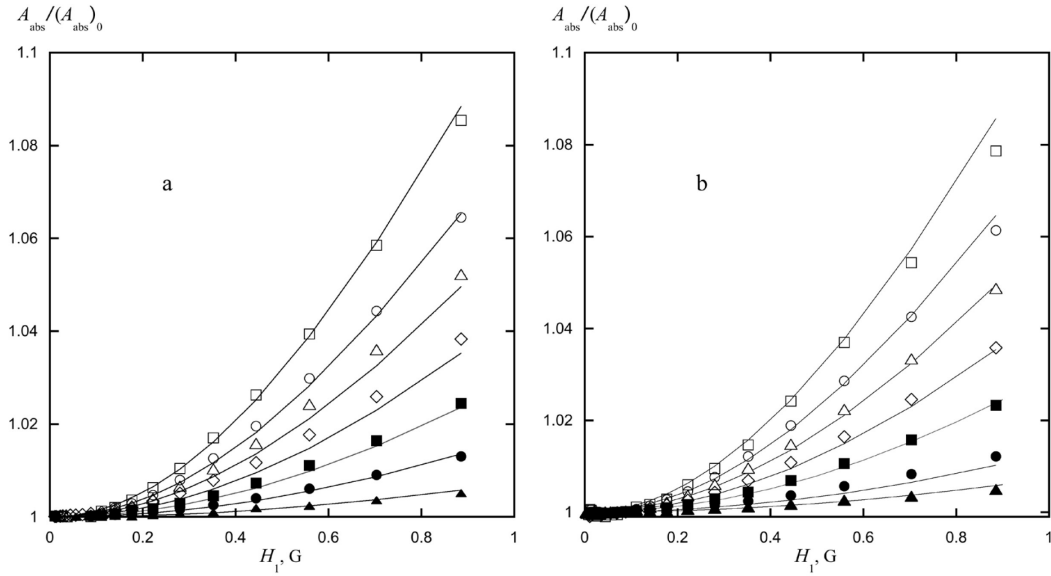

Fig 3 CWS of the normalized line separation. **a** Series 1 and **b** Series 2. $C = 116$ mM, open squares; 98.6, open circles; 82.6, open triangles; 66.0, open diamonds; 49.8, closed squares; 33.3, closed circles; and 18.0, closed triangles. Uncertainties from fitting errors are less than the symbol size. The solid lines are calculated from eq 7 with no adjustable parameters.
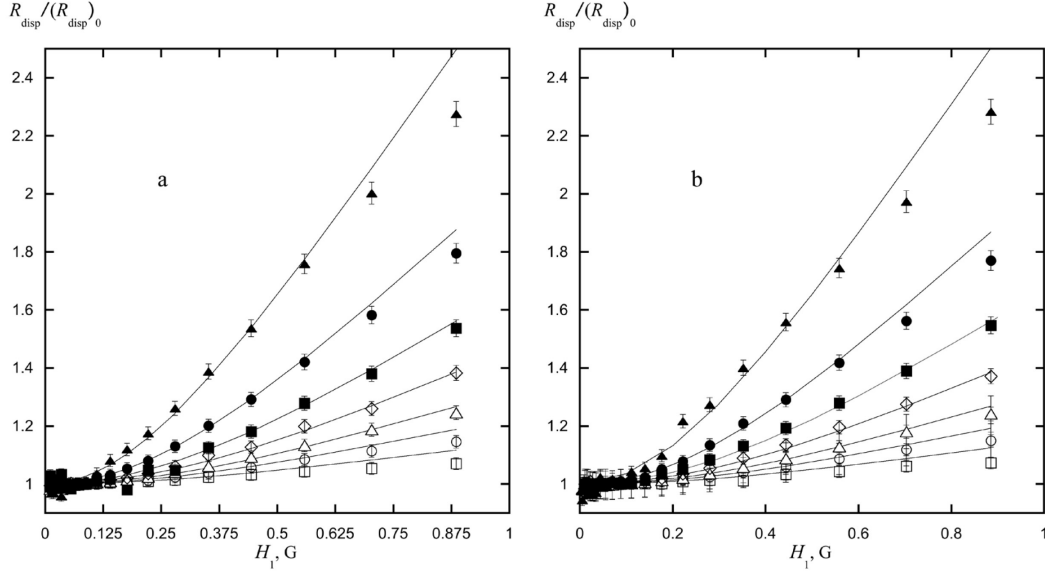
Fig 4 CWS of the normalized DIS contribution. Same symbols as Fig. 3. Uncertainties are estimated from the results of ^{14}N PADS [22], see text. The solid lines are calculated from eq 11 using the same parameters as in Fig. 3 with no adjustable parameters.

Figure 4 shows the H_1 dependence of $R_{disp} \equiv \left(V_{disp}/V_{pp}\right)$. The solid lines are computed from eq 11 using the same parameters as in Fig. 3 with no adjustable parameters. For ^{14}N, no estimate of the uncertainties is available from the two lines, thus, they are estimated to be $\pm$ 1.4 % from experiments with ^{14}N [3]. The agreement is satisfactory although there is an apparent discrepancy at higher values of H_1.
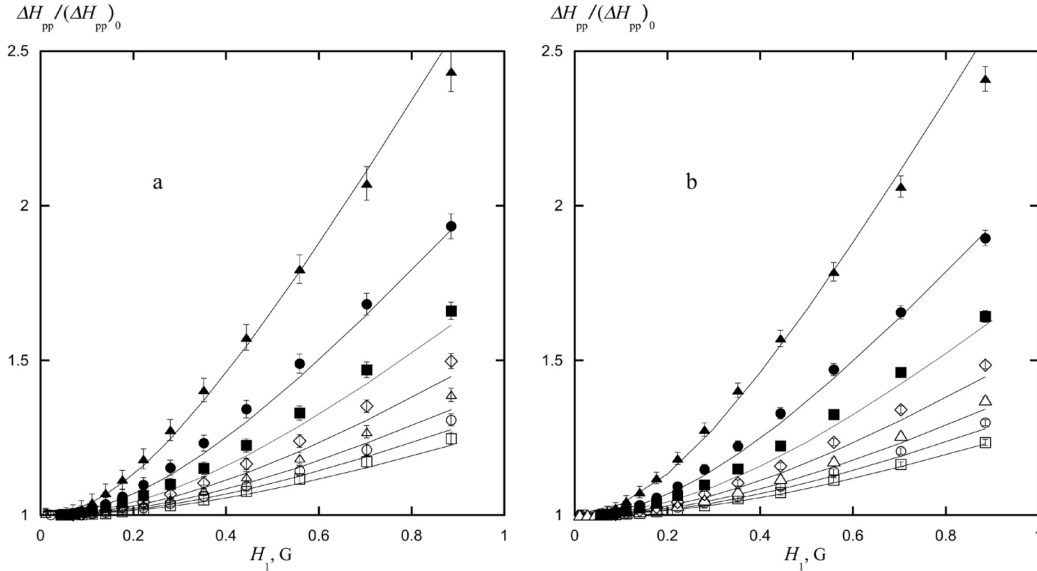

Fig 5 CWS of the Lorentzian line width. Same symbols as Fig 2. Uncertainties are the fit errors of the intercepts of CWS of 0.1 mM 15PADS plus the sd of the difference in lf and hf, taken in quadrature. The solid lines are calculated from eq 10 with no adjustable parameters.

Figure 5 shows the H_1 dependence of ΔH_{pp}^L. The solid lines are computed from eq 10 using the same parameters as in Fig. 3 with no adjustable parameters. The uncertainties are propagated from those for $\left(\Delta H_{pp}^L\right)_0$, Table 2, and the discrepancies in the two values of ΔH_{pp}^L, taken in quadrature. The agreement is satisfactory.

We have not presented results for the peculiar behavior of the doubly-integrated intensity, I, eq 13, because at our maximum value of $H_1 = 0.885$ G, no departure from normal saturation behavior is detectable. The normal behavior is that I increases with H_1 before leveling out to a plateau [9]. Figure 6 shows I in arbitrary units as a function of H_1 where the maximum is not attained at maximum H_1. With this limited information, it is not possible to confirm a peculiar behavior; in fact, the solid lines are best fit to the Bloch equation, eq 11 of [18]. Figure 6 of [9] does show peculiar behavior; however, there, $\gamma T_1 = 20$ G^{-1} which is a factor of about three times longer than we have treated. Also, the range of H_1 up to 3 G is more than three times greater than we have achieved.
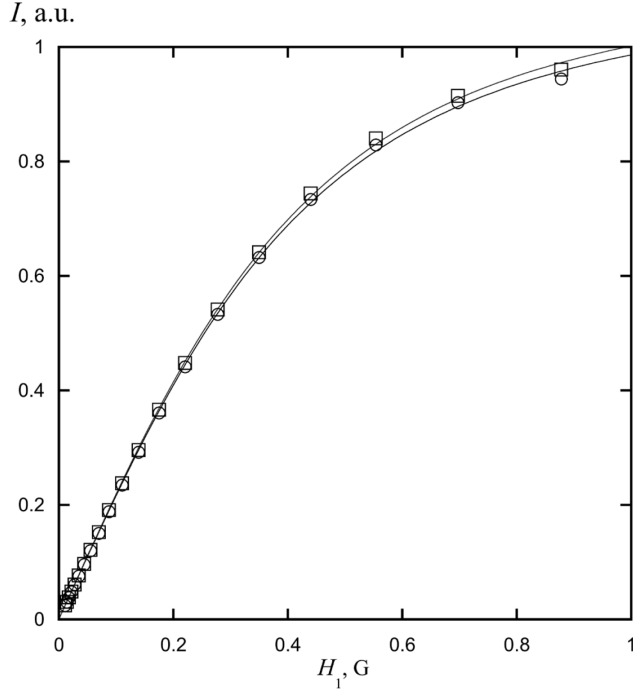

Fig 6 CWS of the doubly integrated intensity of 116 mM 15PADS for Series 2. Circles, lf; squares, hf. Solids lines, fits to Bloch equation. See text.

It is not promising to study I with a commercial spectrometer; however, it might be illuminating to study the saturation of V_{pp} because it varies faster with H_1 [18]. The theoretical prediction for V_{pp} is not explicitly presented in [9]; however, it is easily computed from eqs 10 and 13 as $V_{pp} \propto I / \left(\Delta H_{pp}^L\right)^2$ [10].

5 Conclusions

We have shown that spectra of 15PADS in aqueous 50-mM K$_2$CO$_3$ at 295 K which fulfill the assumptions of the theory that requires two identical Lorentzian lines are in accord with

theory. In particular, the peculiar behavior of the saturation of A_{abs}, previously confirmed to be in accord with theory qualitatively [13, 14], is now confirmed quantitatively. The behavior of ΔH_{pp}^{L} and DIS under saturation, although not obviously peculiar, are also confirmed to be generally correct albeit with discrepancies outside of our estimates of the uncertainties at higher values of H_1.

Declarations

Ethical Approval
Not applicable

Availability of data and materials
Tables 1 and 2 of the manuscript. Any other data by request.

1. J.D. Currin, Phys. Rev. **126**, 1995-2001 (1962)
2. Y.N. Molin, K.M. Salikhov, and K.I. Zamaraev, *Spin Exchange. Principles and Applications in Chemistry and Biology*.(Springer-Verlag, New York, 1980)
3. B.L. Bales and M. Peric, J. Phys. Chem. B **101**, 8707-8716 (1997)
4. D. Marsh, *Spin-Label Electron Paramagnetic Resonance Spectroscopy*.(CRC Press. Taylor & Francis Group, Boca Raton, FL. USA, 2020)
5. B.L. Bales and M. Peric, J. Phys. Chem. A **106**, 4846-4854 (2002)
6. B.L. Bales and M. Peric, Appl. Magn. Reson. **48**, 175-200 (2017)
7. K.M. Salikhov, Appl. Magn. Reson. **47**, 1207 - 1227 (2016)
8. B.L. Bales, M.M. Bakirov, R.T. Galeev, I.A. Kirilyuk, A.I. Kokorin, and K.M. Salikhov, Appl. Magn. Reson. **48**, 1399-1445 (2017)
9. K.M. Salikhov, Appl. Magn. Reson. **52**, 1063-1091 (2021)
10. B.L. Bales, in *Biological Magnetic Resonance*, L.J. Berliner and J. Reuben, Editors. (Plenum, New York, 1989)
11. K.M. Salikhov, Appl. Magn. Reson. **49**, 1417-1430 (2018)
12. K.M. Salikhov, Appl. Magn. Reson. **51**, 297-325 (2020)
13. B.L. Bales, M. Peric, I. Dragutan, M.K. Bowman, M.M. Bakirov, and R.N. Schwartz, J. Phys. Chem. Letters **13**, 10952-10957 (2022)
14. K.M. Salikhov, M.M. Bakirov, R.B. Zaripov, and I.T. Khairutdinov, Phys. Chem. Chem. Phys. **25**, 17966-17977 (2023)
15. K.M. Salikhov, *Fundamentals of Spin Exchange. Story of a Paradigm Shift*.(Springer, Switzerland, 2019)
16. B.L. Bales, M. Peric, and R.N. Schwartz, J. Phys. Chem. Lett. **15**, 2082-2088 (2024)
17. B.L. Bales, M. Peric, D. Kinzek, and R.N. Schwartz, J. Magn. Reson. **351**, 107456 - 107459 (2023)
18. M.M. Bakirov, K.M. Salikhov, M. Peric , R.N. Schwartz, and B.L. Bales, Appl. Magn. Reson. **50**, 919-942 (2019)

19. B.L. Bales, E. Wajnberg, and O.R. Nascimento, J. Magn. Reson. **A 118**, 227-233 (1996)
20. B.L. Bales, M. Meyer, S. Smith, and M. Peric, J. Phys. Chem. *A* **112**, 2177-2181 (2008)
21. M.P. Eastman, G.V. Bruno, and J.H. Freed, J. Chem. Phys. **52**, 321-327 (1970)
22. B.L. Bales, M. Meyer, S. Smith, and M. Peric, J. Phys. Chem. *A* **113**, 4930-4940 (2009)